A STUDY ON THE CALIBRATION OF AN HPM METER BASED ON A D-DOT SENSOR AND LOGARITHMIC RF POWER DETECTOR

Jacek Jakubowski

Military University of Technology, Faculty of Electronics, Institute of Electronic Systems, gen. S. Kaliskiego 2, 00-908 Warsaw, Poland (✉ *jacek.jakubowski@wat.edu.pl*, +42 261 837 937)

Abstract

HPM meters are required for the assessment of fields generated by sources of high-power microwaves. Finding the inverse calibration curves for such instruments is important for ensuring accuracy. The procedure is relatively simple for meters consisting of linear devices but there can also be hardware solutions implementing nonlinear ones. The objective of the present work was to develop a convenient procedure to allow finding such a curve when the meter uses a D-dot probe and a power detector. For that purpose, the results of low voltage measurements describing the properties of the detector were first analysed. Then a software code was developed to estimate the RMS value of an incident field based on measured output and frequency response. The response was estimated with very low electric field. And finally, the performance of the proposed procedure was verified by tests conducted with high electric field in a TEM cell. High conformity of the output of the meter with fields of known values was demonstrated. The maximum error related to the meter range did not exceed 4%.

Keywords: HPM measurements, sensor calibration, RF detector, D-dot sensor.

1. Introduction

Nowadays, non-nuclear devices with powerful batteries capable to *radiate high-power microwave* (HPM) pulses strong enough to remotely upset or even damage numerous systems of critical infrastructure are easily available. Because of that the threat of their intentional use as a means of terroristic attacks is faced by many protection authorities [1, 2]. In the last decade simply a new term arose – electromagnetic terrorism [3], used to report illegal or criminal attempts to interfere with operation of modern electronic microcircuits and to disrupt or disable computer software. Fortunately, the development of these non-lethal HPM weapons has brought a considerable improvement in the immunity of critical systems to them. The susceptibility of the systems to penetrating HPM fields depends on the level of electromagnetic shielding available from a building as well as from that provided by dedicated enclosures made of materials of sufficient transmission loss [4, 5]. Because of the necessity to describe the required attenuation quantitatively as well as characteristic parameters of the HPM signal itself, including

field strength, pulse width and repetition, the measurement methods of such high-frequency and transient electromagnetic phenomena receive great concern.

One way to measure the phenomena is using electric field sensors with constant frequency response over the band as wide as possible to satisfy possible HPM spectrum variations. Some of commercially available sensors, fulfilling this requirement in the frequency range up to several gigahertz and more, work as passive differential sensors, *i.e.* their output voltage is proportional to the time derivative of the incident input electric field [6]. They are called D-dot sensors where the "dot" emphasizes the differentiation of the electric field D. In principle, integration is an indispensable part of the processing of a D-dot output to recover the waveform shape of the field. The sensors meet the requirement of good linearity and high sensitivity; however, some additional activity must be performed to ensure high-voltage isolation preventing a measuring system in the chain from damage. Besides, the relationship between output voltage and electric field must also be established to achieve reliable measurements in finding the actual field strength. The procedure for that must be performed while making a measuring instrument and differs from the routine procedure of calibration carried out during the type approval tests. Therefore, it is sometimes called primary calibration [7]. In most cases, the measuring chain consists of linear elements and devices and such calibration procedure is relatively simple but, in some others, they are nonlinear. This paper deals with the problem of establishing the relationship between the input and output of an HPM meter containing a non-linear *radio frequency* (RF) detector to find the strength of the HPM pulse envelope instead of the HPM wave itself.

2. Related works

Traditional application of the D-dot sensor in HPM measuring sets is based on the analysis of its output waveforms representing electrical fields. Acquisition of the waveforms became possible thanks to the advent of fast *analogue to digital converters* (ADC). The converters with sampling frequencies of up to 50 GHz are applied in modern digital scopes which, thanks to that, are used as front ends of many measuring sets [6, 8–10]. In sets especially intended to measure strong fields, there arises the problem of the measuring data transmission. Commonly used coaxial cables are vulnerable to electromagnetic penetration and the longer the distance from the measuring volume to the low voltage acquisition system, the more degraded is the high frequency signal. Because of that, an optical fibre transmission link is recommended [11, 12]. The transmitter of the link converts electrical signal from the sensor after attenuation into an optical one and the receiver restores the signal transmitted through the optical fibre again to the electrical domain. The simplified diagram of such meters is depicted in Fig. 1.
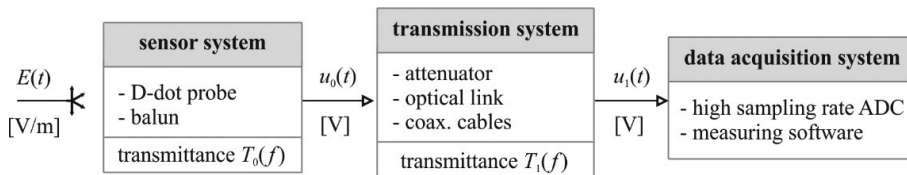
Fig. 1. Block diagram of a typical HPM meter.

In the case of free field measurements, the sensor requires a balanced-to-unbalanced transformer (balun) on its output. To assess the field $E(t)$ on the basis of the voltage waveform $u_1(t)$

acquired by an oscilloscope or another fast ADC converter, a correction must be taken into account according to the following equation:

$$E(t) = C_f \cdot u_{1(\text{int})}(t), \tag{1}$$

where $u_{1(\text{int})}(t)$ is the integral of the output voltage of the analogue part of the measuring chain. The properties of the chain are expressed numerically by the correction factor C_f which depends on the matching impedance, the equivalent area of the probe and overall attenuation introduced by the balun converter, optical link, attenuator and cables. When the sampling frequency is high enough, the integration of the acquired signal can be performed numerically with the use of a digital filter approximating the transmittance of an integrated circuit $1/s$ according to Tustin's or Simpson's methods [6]. However, care must be taken because possible signal offset can significantly degrade computations in numerical integration. It should be prior adjusted to avoid errors [13, 14].

The above correction coefficient can be found either theoretically, according to the recommendations of the manufacturer of the measuring chain [12], or experimentally by means of calibration with the use of a field generator tailored to the frequency range of the meter. The manufacturer's recommendations are determined from measured physical properties and electrical characteristics of used elements and devices. If the meter is assumed to be linear, then the experimental calibration can be performed in lower fields because the only limiting nonlinear factor is simply the electrical flashover. This property is of fundamental importance as HPM meters are very often intended to measure strong fields that are usually unavailable in laboratory conditions. In many reported calibration procedures, as for example in [8, 15, 16], the sensor is placed in a reference pulsed field and the correction factor is adjusted so as to fit the integral waveform of the acquired voltage $u_{1(\text{int})}(t)$ to the known waveform of the field $E(t)$. Calibration can also be performed using continuous wave excitation at one or more frequencies, according to recommendations given in IEEE standard 1309-2013 [17].

3. Proposed approach

The frequency band of many meters consisting of linear elements and devices can be seriously limited by lack of an ADC converter with sufficient analogue bandwidth and sampling frequency [18]. Scopes with sampling reported earlier in this paper are rather expensive. Besides, they are usually too bulky to be of any use in field measurements as portable instruments. To retain the possibility to measure HPM pulses based on AM modulation with high carrier frequencies, the diagram of the meter depicted in Fig. 1 can be modified with the use of one of the RF power detectors. The detectors can output envelope signals with bandwidth narrow enough (ca. 100 MHz for pulses of duration several nanoseconds) that even middle-class ADC converters or scopes with analogue bandwidth of merely 300 MHz and sampling of 1 GHz can handle the acquisition. In this paper, the research on finding the relationship between electric field and the output of an HPM meter based on an HMC948LP3E logarithmic RF amplifier working in conjunction with a commercially available D-dot sensor, optical link and autonomous ADC is reported. The amplifier was adopted to fit the ±0.5 V input range and impedance of the ADC converter as described in [19]. The resulting meter, presented in Fig. 2, enables measuring HPM pulses of a carrier frequency of up to 12 GHz which is over four times higher than the analogue bandwidth of the ADC converter.

The HMC948LP3E model is a complete monolithic demodulating logarithmic amplifier based on the successive compression technique providing a 54 dB dynamic range from 1 to 23 GHz.
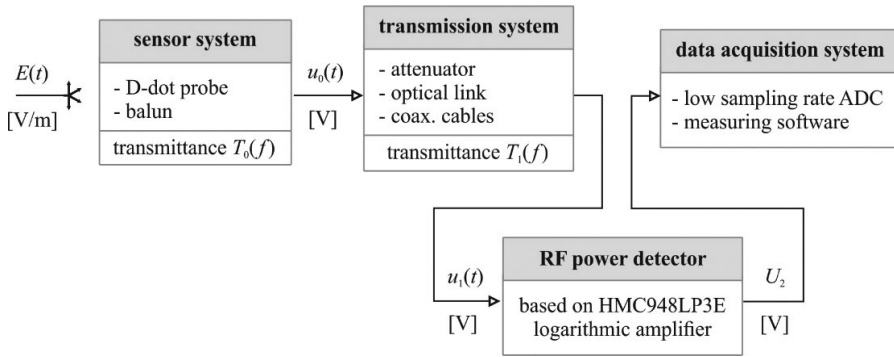
Fig. 2. Block diagram of an HPM meter with a power detector in the measuring chain.

Similarly to many others, its output DC voltage in ideal case should be proportional to the input power expressed in dBm or to the logarithm of the input voltage as depicted in Fig. 3.
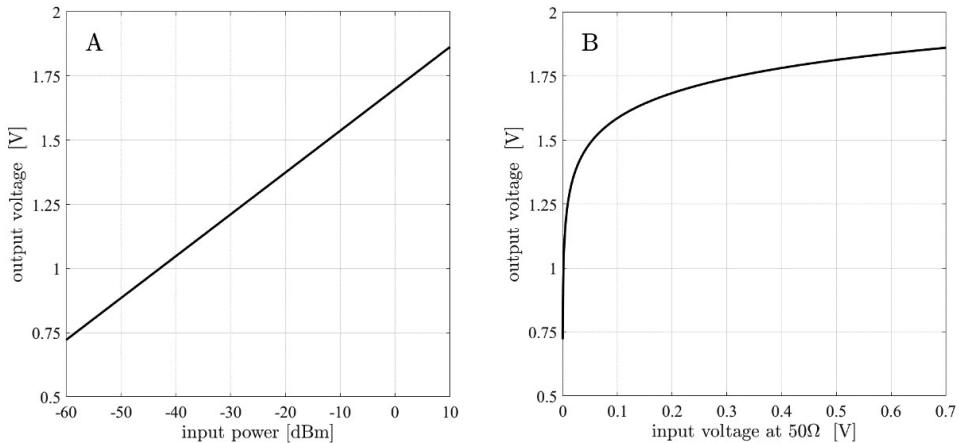
Fig. 3. Conversion characteristics of a hypothetical ideal logarithmic power detector:
A – power as the input quantity, B – voltage as the input quantity.

If the type of the function describing the conversion characteristic of the power detector were known in advance, calibration of the meter at very high field strengths would not be necessary, just like in linear cases. The parameters of the conversion required to find the inverse model could be then estimated by means of approximation based only on a few data points corresponding to several fields of low strength. The problem is that the conversion characteristic of a real detector is not ideal and it is very difficult to find an appropriate function that could be identified in lower fields to approximate the inversion model precisely enough to predict strong fields which are characteristic for real HPM sources. Literally, the meter response to strong fields should be then found and used to produce a table to find the result of the measurement in final use conditions [17]. Because of possible dependence of the conversion on frequency, such strong-field measurements should be performed for the whole frequency range of the meter. However, additional laboratory measurements, just like these reported in this paper, allow us to avoid this inconvenient calibration in high-frequency fields.

3.1. Results of laboratory measurements

The laboratory measurements were performed to find the properties of the HMC948LP3E based detector after its adaptation to the ADC converter input and covered input-output characteristic and frequency response. The measurements were performed with R&S®SMB100A and SMF100A microwave signal generators to get signal pulses of adjustable amplitude with carrier frequency ranging from 1 GHz to 12 GHz. The output of the detector was acquired by an ADQ7 Teledyne SP Devices ADC converter [20]. In order to get reliable results, long pulses of duration 10 microseconds and averaging of the samples corresponding to the top of a pulse were used. The results of measurements are depicted in Fig. 4.
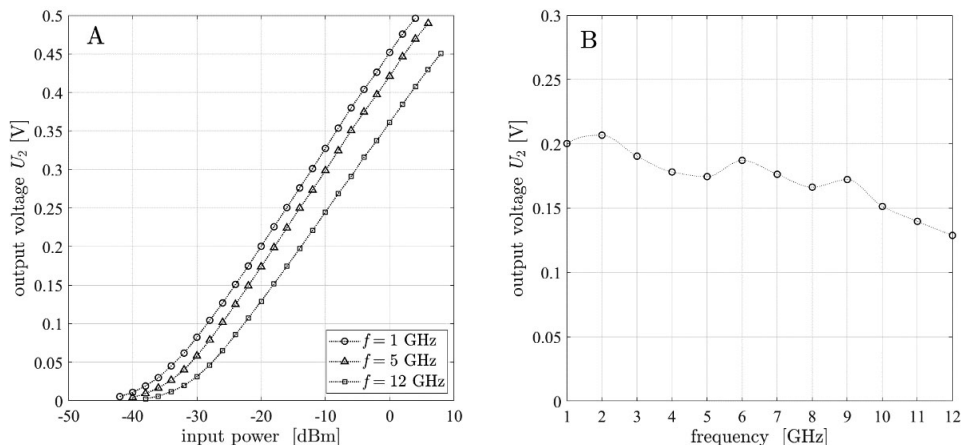
Fig. 4. Results of measurements describing the power detector used in this work:
A – conversion characteristics, B – frequency response for the excitation power of –20 dBm.

As it can be seen in the figure, the conversion characteristics of the detector are not linearly related to the logarithm of input power. In practice, the inverted characteristics are required [7] as they enable finding the input of the detector based on the measured output voltage. The inverted characteristics could be quite well approximated by polynomial models of sufficient orders. The results of such approximations for the case of 1 GHz are presented in Fig. 5.

Table 1 shows the models explicitly together with the values of the basic measure – mean absolute error (MAE), recommended for assessing average model performance of any fit with the mean of the absolute value of the residuals [21]. The orders of the models were chosen on the basis of the χ^2-test as the lowest orders at which the test did not disprove the hypothesis that the corresponding polynomial is in agreement with experimental data [22]. Linear piecewise, cubic or spline interpolation can also be used to predict data between experimental points.

Table 1. Polynomial models describing inverted characteristics of the RF power detector used in this stude.

Inverted characteristic	Model for 1 GHz	MAE
input power P_1 vs. output DC voltage U_2	$\hat{P}_1 = (2.1065 \cdot U_2^7 - 4.063 \cdot U_2^6 + 3.182 \cdot U_2^5 - 1.299 \cdot U_2^4 +$ $+0.2959 \cdot U_2^3 - 0.03759 \cdot U_2^2 + 0.003319 \cdot U_2 - 0.0004339) \cdot 10^5$	0.1 dBm
input RMS voltage U_1 vs. output DC voltage U_2	$\hat{U}_1 = 52.4251 \cdot U_2^5 - 46.6057 \cdot U_2^4 + 17.0606 \cdot U_2^3 +$ $-2.3396 \cdot U_2^2 + 0.1852 \cdot U_2 + 0.0002$	0.9 mV
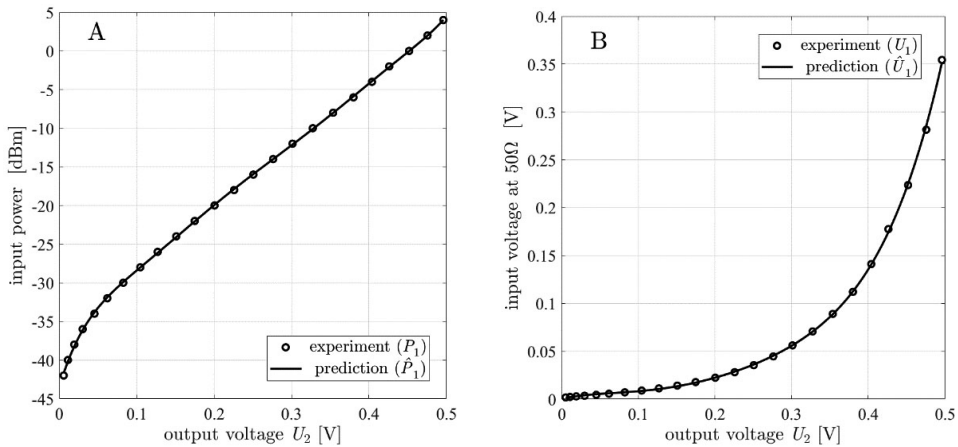
Fig. 5. Inverted conversion characteristics of the power detector used in this study for 1 GHz excitation:
A – input power as the dependent variable, B – input voltage as the dependent variable.

3.2. Construction of the inverse calibration curve of the meter

Let us assume that the D-dot sensor of the meter presented in Fig. 2 is exposed to an incident electric pulsed field of 1 GHz carrier frequency and strength E and try to analyse propagation of the signal from end to front. The field will bring a certain output DC voltage U_2, measured by the ADC converter. The corresponding RMS value of the input voltage u_1 of the detector can be predicted as $\hat{U}_1(U_2)$, *i.e.* with the polynomial model from Table 1, describing the inverted characteristic. The u_1 voltage is the output of the transmission system with transmittance $T_1(f)$, so one can also easily predict the RMS of its input voltage as:

$$\hat{U}_0 = \frac{\hat{U}_1(U_2)}{|T_1(1\,\text{GHz})|} \,. \tag{2}$$

If there is an attenuator in the measuring chain with fixed attenuation A [dB], then the voltage can be expressed as:

$$\hat{U}_0 = \frac{\hat{U}_1(U_2)}{|T_1(1\,\text{GHz})| \cdot 10^{-A/20}} \,. \tag{3}$$

Voltage u_0 is the output of the sensor system of transmittance $T_0(f)$, so the RMS of its input can be estimated as:

$$\hat{E} = \frac{\hat{U}_0}{|T_0(1\,\text{GHz})|} = \frac{\hat{U}_1(U_2)}{|T_0(1\,\text{GHz})| \cdot |T_1(1\,\text{GHz})| \cdot 10^{-A/20}} = \frac{\hat{U}_1(U_2)}{|T(1\,\text{GHz})| \cdot 10^{-A/20}} \,, \tag{4}$$

where $|T_0(1\,\text{GHz})|$ is the module of the overall transmittance of the sensor and transmission systems for the frequency of 1 GHz, expressed in [V/kVm^{-1}]. From the last equation one can find that with pairs of real measurements (E, U_2) performed during calibration for different frequencies, it is possible to estimate the module of overall transmittance:

$$\left|\hat{T}(f)\right| = \frac{\hat{U}_1(U_2)}{E(f) \cdot 10^{-A/20}} \,, \tag{5}$$

which, in turn, can be used in (4) to find the strength of the field on the basis of the corresponding measured U_2 value:

$$\hat{E}(f) = \frac{\hat{U}_1(U_2)}{\left|\hat{T}(f)\right| \cdot 10^{-A/20}} \ . \tag{6}$$

And what is most important – the module of the transmittance $T(f)$ can be estimated according to (5) with the field of any strength but, of course, low strengths are of particular interest. On the other hand, once estimated, it can be used according to (6) to find the strength of any field, including strong fields existing in the HPM domain.

3.3. Examination of the nonlinearity

However, there is certain inaccuracy in the above construction that should be explained and made less severe. The construction assumes that the nonlinearity of the power detector is not dependent on the frequency. Such dependence is, however, observed in the results of experiments depicted in Figs. 4 and 5 but may be exclusively caused by a linear, frequency dependent filter-like circuit formed by parasitic capacitances with output voltage u_x as depicted in Fig. 6.
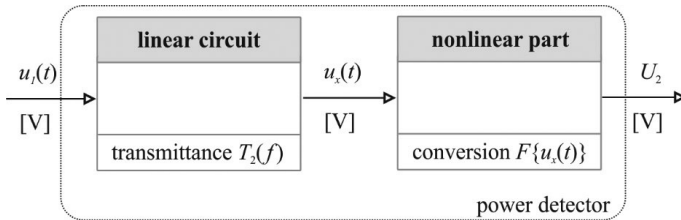
Fig. 6. Block diagram of the power detector used to examine its nonlinearity.

If this is true, then the transmittance $T_2(f)$ of the circuit can be considered as part of the overall transmittance and no change in the above construction is necessary. To examine more deeply the observed dependence on the frequency, let us consider two excitations of frequencies 1 GHz and 12 GHz. The equations, describing the processing of RMS values of such excitations in the circuit depicted in Fig. 6, are as follows:

$$U_x(1\,\text{GHz}) = U_1(1\,\text{GHz}) \cdot |T_2(1\,\text{GHz})| = F^{-1}\{U_2(1\,\text{GHz})\}, \tag{7}$$

$$U_x(12\,\text{GHz}) = U_1(12\,\text{GHz}) \cdot |T_2(12\,\text{GHz})| = F^{-1}\{U_2(12\,\text{GHz})\}, \tag{8}$$

where F is the conversion characteristic of the pure nonlinear part of the detector. If the conversion F is not frequency dependent, then for equal output voltages:

$$U_2(1\,\text{GHz}) = U_2(12\,\text{GHz}), \tag{9}$$

the input voltages will also be equal:

$$U_x(1\,\text{GHz}) = U_x(12\,\text{GHz}). \tag{10}$$

And thus, according to (7) and (8):

$$U_1(1\,\text{GHz}) \cdot |T_2(1\,\text{GHz})| = U_1(12\,\text{GHz}) \cdot |T_2(12\,\text{GHz})|, \tag{11}$$

$$U_1(12\,\text{GHz}) = \frac{|T_2(1\,\text{GHz})|}{|T_2(12\,\text{GHz})|} \cdot U_1(1\,\text{GHz}) = K \cdot U_1(1\,\text{GHz}). \tag{12}$$

The relation described by the last equation can be examined using inverted conversion models for these two frequencies $\hat{U}_1^{12\,\text{GHz}}$ and $\hat{U}_1^{1\,\text{GHz}}$, which are based on experimental data, to check if there is a scaling constant K giving:

$$\hat{U}_1^{12\,\text{GHz}}(U_2) = K \cdot \hat{U}_1^{1\,\text{GHz}}(U_2). \tag{13}$$

for a set of observed U_2 values. The examination was based on linear piecewise interpolation models for both frequencies and led to the determination of the scaling constant K that minimized the MAE error between both sides of (13) for a vector of values taken from the range of U_2 in real measurements presented in Fig. 4. The best result of such scaling, achieved for $K_{opt} = 2.29$, is depicted in Fig. 7. As can be seen, the fitting is not perfect as the models are slightly shifted. If the observed non-linearity were not frequency dependent, then model explaining it for 1 GHz after scaling should be also valid for 12 GHz.
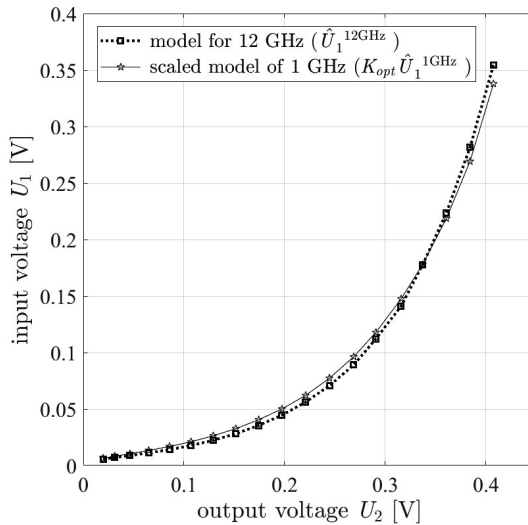
Fig. 7. Fitting the inverse conversion model of the detector for 1 GHz to the model for 12 GHz.

So, the nonlinearity is rather frequency dependent and the formulas for the transmittance and inverse calibration curve, described by (5) and (6), should be modified to take into account the new input quantity:

$$\left|\hat{T}(f)\right| = \frac{\hat{U}_1(U_2, f)}{E(f) \cdot 10^{-A/20}}, \tag{14}$$

$$\hat{E}(f) = \frac{\hat{U}_1(U_2, f)}{\left|\hat{T}(f)\right| \cdot 10^{-A/20}}. \tag{15}$$

The numerator in the above equations is thus a surface that can be modelled with the use of a set of conversion characteristics of the power detector measured for several frequencies of excitation with ordinary measuring instruments described in section 3.1. The model based on linear piecewise interpolation, when the results of laboratory measurements depicted in Fig. 4 were used, is shown in Fig. 8.
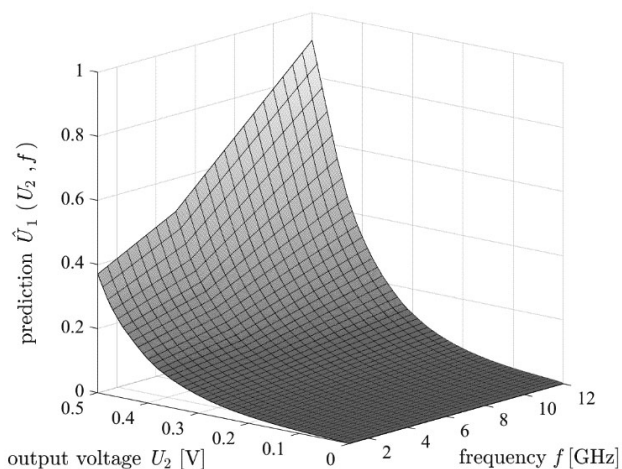
Fig. 8. Final inverse conversion model of the detector used in this work.

To find the prediction of the input voltage for a detector based on known output voltage U_{2x} and frequency f_x, two steps of intermediate prediction should be performed. First, possible n predictions of input voltages U_f for a measured output voltage U_{2x} have to be found on the basis of n experimental curves $(U_1$ vs. $U_2)_f$ corresponding to n frequencies:

$$
\begin{aligned}
U_f(1) &= \text{prediction}\left\{(U_1 \text{ vs. } U_2)_{f1}, U_{2x}\right\}, \\
U_f(2) &= \text{prediction}\left\{(U_1 \text{ vs. } U_2)_{f2}, U_{2x}\right\}, \\
&\vdots \\
U_f(n) &= \text{prediction}\left\{(U_1 \text{ vs. } U_2)_{fn}, U_{2x}\right\}.
\end{aligned}
\tag{16}
$$

Next, the second step of prediction comes which takes into account the signal frequency f_x:

$$
\hat{U}_1(U_{2x}, f_x) = \text{prediction}\left\{\left(U_f \text{ vs. } f\right), f_x\right\},
\tag{17}
$$

Alternatively, a look-up table can be established in advance on the basis of ADC codes and possible frequency values. Prediction in the above equations can be performed on the basis of models developed by approximation or interpolation.

4. Experimental verification

The construction of the inverse calibration curve of the presented HPM meter, described by (15) above, was verified by a certified laboratory that is able to generate electric fields of known values and frequencies. First, the frequency response of the meter in the range from 1 GHz to 12 GHz was measured with excitation pulses of 5 μs length and 1 ms repetition. Such broadband conditions of excitation were obtained in an anechoic chamber with the use of a horn antenna. The calibration RMS value of the excitation field in a single pulse was assumed to be extremely low in accordance with the general idea presented in this paper and was set to 20 V/m. The results of measurements as well as the module of transmittance of the linear part of the meter estimated with the use of (14) and (17) for the case of 0 dB attenuator are jointly presented in Fig. 9.

681
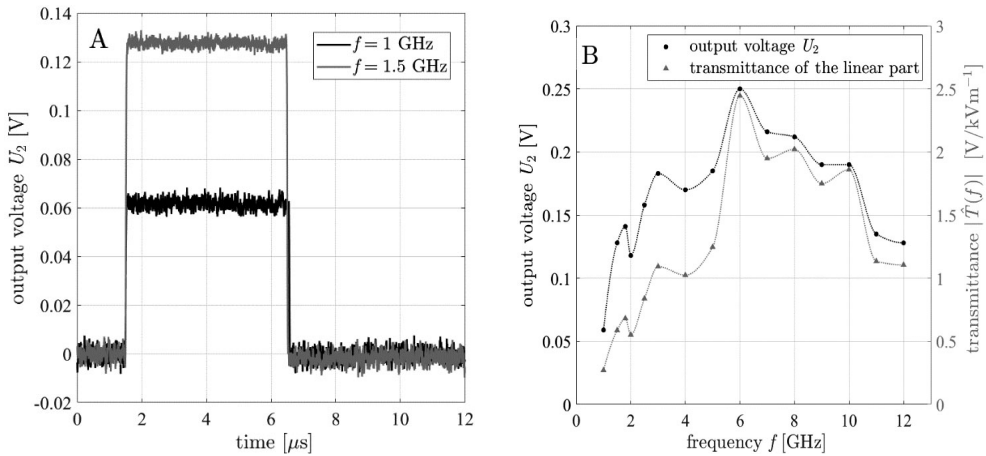
Fig. 9. Results of measurements and processing for the case of 20 V/m free field excitation in the frequency range 1–12 GHz: A – output pulses acquired by the ADC converter for two exemplary frequencies, B – output of the meter as a function of frequency together with the module of transmittance of its linear part.

As can be seen, the shape of the transmittance differs from the shape of the frequency response as the latter is the effect of the nonlinearity which additionally depends on frequency (see section 3.1). The module of the transmittance was measured for a finite set of frequencies, but interpolation methods enable finding its values for other frequencies as well. After this step of measurements, the meter is ready to use as all components required for computations according to the inverse calibration curve in (15), including the inverse conversion model of the detector, are available. The readiness of the meter for proper measurements of HPM fields, much higher than 20 V/m used in the above experiment, was then further verified by placing the D-dot sensor in a transverse electromagnetic cell (TEM) following recommendations given in the IEEE standard for calibration of field sensors [17]. The cell was able to generate 1 GHz pulse fields of values high enough to reach the dynamic range of the ADC converter as depicted in Fig. 10A where the output of the power detector is presented as a function of known RMS value of the incident electric field. The corresponding field values calculated according to (15) as final results of measurements are depicted in Fig. 10B as "experiment".

The value close to the full scale of the ADC converter was reached when the RMS of the input field was 1.2 kV/m. The measurements were performed with the 0 dB attenuator, so the field value can be treated as the lowest subrange of the meter $E_{1\,\text{max}}$. Higher subranges will depend on the attenuators used. The experimental result presented in Fig. 10B was assessed by finding the linear fit without the intercept factor and only with the slope that in the ideal case should be $a = 1$. The statistics describing the experiment are summarized in Table 2.

Table 2. Measures assessing the inverse calibration curve of the HPM meter.

Estimated slope with standard deviation $\hat{a} \pm \hat{\sigma}_{\hat{a}}$	99% confidence bounds for the slope	Coefficient of determination R^2	Mean absolute error MAE	Maximum absolute error $\Delta_{\text{max}} = \max\left\{\left|E_i - \hat{E}_i\right|\right\}$	Maximum absolute error $\delta = \dfrac{\Delta_{\text{max}}}{E_{1\,\text{max}}}$
0.991 ± 0.004	0.979–1.003	0.9992	5 V/m	44 V/m	3.7%
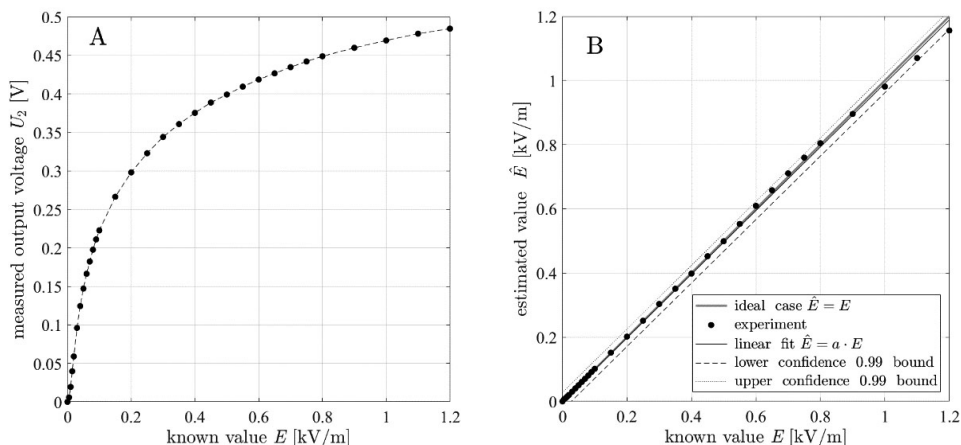
Fig. 10. Results verifying the ability of the meter to measure high electric fields of values not used in calibration:
A – conversion characteristic with the raw output, B – results of processing performed to indicate the measured field.

As can be seen, the interval defined by the 99% confidence bounds for the slope contains the ideal value of 1. The ideal fit depicted in Fig. 10B also lies within the 99% confidence region and high value of the coefficient of determination indicates a good fit of the linear model to experimental data.

5. Conclusions

In the present work, an algorithm establishing the relationship between the RMS value of incident electric field and output DC voltage of the HPM meter using a power detector in the measuring chain was proposed and discussed. The algorithm is based on the properties of the power detector derived from low voltage measurements of its conversion characteristics performed for different frequencies. The results of conducted research indicate that the nonlinearity of the detector depends on frequency. The algorithm requires measuring the frequency response of the meter to identify the module of overall transmittance of its linear part including the transmittance of the sensor system and transmission system; however, no high calibration fields of different frequencies are necessary to take into account the observed dependence of the nonlinearity of the detector on frequency. The field used to find the frequency response of the meter was merely 20 V/m but verification experiments realized in a TEM cell showed that the meter was able to measure calibration fields of up to 1.2 kV/m (without an external attenuator). The statistics presented in the previous section indicate that the results of such measurements seem to be quite satisfactory – mean absolute error was 5 V/m and the maximum error related to the meter range did not exceed 4 %. It should be remembered that presented algorithm assumes that the frequency of the field is known in advance. In general, it does not pose a problem as the frequency is known indeed in many electromagnetic compatibility applications or can be successfully measured *e.g.* with a ring phase-sensitive detector [23].

Acknowledgements

from HPM pulses" and was devoted to the task "*The concept of a portable instrument for measurements of high power electromagnetic fields*".

References

[1] Hamamah, F., Ahmad, W. W., Gomes, C., Isa, M. M., & Homam, M. (2019). Concerns on the Risk of Malaysian Civil and Defense Systems Due to Intentional Electromagnetic Interference. *IEEE Asia-Pacific Conference on Applied Electromagnetics (APACE)*, Malaysia. https://doi.org/10.1109/APACE47377.2019.9021096

[2] Lanzrath, M., Adami, C., Joerres, B., Lubkowski, G., Joester, M., Suhrke, M., & Pusch, T. (2017). HPEM vulnerability of smart grid substations coupling paths into typical SCADA devices. *International Symposium on Electromagnetic Compatibility – EMC EUROPE*, Angers, 1–6. https://doi.org/10.1109/EMCEurope.2017.8094632

[3] Radasky, W. A., & Bäckström, M. (2014). Brief historical review and bibliography for Intentional Electromagnetic Interference (IEMI). *XXXIth URSI General Assembly and Scientific Symposium (URSI GASS)*, Beijing, 1–4. https://doi.org/10.1109/URSIGASS.2014.6929517

[4] Radasky, W. A. (2010). Protection of commercial installations from the high-frequency electromagnetic threats of HEMP and IEMI using IEC standards. *Asia-Pacific International Symposium on Electromagnetic Compatibility*, Beijing, 758–761. https://doi.org/10.1109/APEMC.2010.5475520

[5] Voicu, V., Pătru, I., Nicolae, P., & Dina, L. (2017). Analyzing the attenuation of electromagnetic shielding materials for frequencies under 1 GHz. *10th International Symposium on Advanced Topics in Electrical Engineering (ATEE)*, Bucharest, 336–339. https://doi.org/10.1109/ATEE.2017.7905057

[6] Zhang, H., Zhou, Y., Shi, L., Ma, R., & Huang, Z. (2014). Design of Electric Field Sensors for Measurement of Electromagnetic Pulse. *Sensors & Transducers, 162*(1), 131–135.

[7] Granovski, V., & Siraia, T. (2013). Direct and Inverse Calibration Curves of Measuring Instruments: Selection and Fitting. *16th International Congress of Metrology, published by EDP Sciences*, France. https://doi.org/10.1051/metrology/201304006

[8] Yunsheng, J., & Cui, M. (2017). Research on calibration accuracy of D-Dot transient electric field sensor. *IEEE Conference on Antenna Measurements & Applications (CAMA)*, Tsukuba, 69–71. https://doi.org/10.1109/CAMA.2017.8273480

[9] Przesmycki R., & Bugaj M. (2019). D-dot Probes Used in HPM Pulse Measurements. *PhotonIcs & Electromagnetics Research Symposium – Spring (PIERS-Spring)*, Italy, 3126–3134. https://doi.org/10.1109/PIERS-Spring46901.2019.9017522

[10] Sanjay, D.R., Chourasia, N., & Singh, R.K. (2019). Experimental study of factors affecting the High Power Microwave measurements. *2019 IEEE Asia-Pacific Microwave Conference (APMC)*, Singapore, 877–879. https://doi.org/10.1109/APMC46564.2019.9038685

[11] Zhang, G, Li, W, Qi, L, Liu, J, Song, Z, & Wang, J. (2018). Design of Wideband GHz Electric Field Sensor Integrated with Optical Fiber Transmission Link for Electromagnetic Pulse Signal Measurement. *Sensors (Basel), 18*(9). https://doi.org/10.3390/s18093167

[12] Sallin, M., & Daout, B. *Derivative time-domain sensor and fiber optic correction factor calculation*. [Montena Technical Notes TN15], Switzerland. https://www.montena.com/fileadmin/technology _tests/documents/technical_notes/TN15E_Sensor_correction_factor.pdf.

[13] Daout, B. *Adjustment of the offset when using the integration function on a scope* [Montena Technical Notes TN27], Switzerland. https://www.montena.com/fileadmin/technology_tests/documents/ technical_notes/TN27B_offset_adjustment_using_integral_function.pdf.

[14] Yao, L., Huang, J., Kang, N., Shen, T., Liu, D., Zhang, F., & Sun, H. (2014). Compensation of the offset in numerical integration of a D-dot sensor measurement. *Proceedings of 2014 3rd Asia-Pacific Conference on Antennas and Propagation*, Harbin, 898–901. https://doi.org/10.1109/APCAP.2014.6992645

[15] Jiang, Y., & Meng, C. (2019). Calibration Method Research for High Power Transient Electromagnetic Field Sensor. *IEEE Conference on Antenna Measurements & Applications (CAMA)*, Indonesia, 1–4. https://doi.org/10.1109/CAMA47423.2019.8959615

[16] Wang, K., Duan, Y., Shi, L., & Qiu, S. (2019). Laboratory Calibration of D-dot Sensor Based on System Identification Method. *Sensors, 19*(15), 3255. https://doi.org/10.3390/s19153255

[17] IEEE Standard for Calibration of Electromagnetic Field Sensors and Probes (Excluding Antennas) from 9 kHz to 40 GHz. (2013). *IEEE Std 1309-2013 (Revision of IEEE Std 1309-2005)*. https://doi.org/10.1109/IEEESTD.2013.6673999

[18] Achtenberg, K., Mikołajczyk, J., Szabra, D., Prokopiuk, A., & Bielecki, Z. (2020). Review of peak signal detection methods in nanosecond pulses monitoring. *Metrology and Measurement Systems, 27*(2), 203–218. https://doi.org/10.24425/mms.2020.132770

[19] Kuchta, M., & Białek, R. (2020). Envelope converter for amplitude-modulated high-frequency signals. *Przegląd Elektrotechniczny, 96*(2), 150–153. https://doi.org/10.15199/48.2020.02.36

[20] Teledyne SP Devices. (June 2020). ADQ7DC Datasheet. https://www.spdevices.com/products/hardware/14-bit-digitizers/adq7dc.

[21] Willmott, C.J., & Matsuura, K. (2005). Advantages of the mean absolute error (MAE) over the root mean square error (RMSE) in assessing average model performance. *Climate Research, 30*(1), 79–82. https://doi.org/10.3354/cr030079

[22] Brandt, S. (2014). *Data Analysis: Statistical and Computational Methods for Scientists and Engineers*. Springer International Publishing. https://doi.org/10.1007/978-3-319-03762-2

[23] Rećko, C. & Stec, B. (2018). Modification of microwave frequency detector characteristic with the use of phase shifter. *Metrology and Measurement Systems, 25*(4), 769–777. https://doi.org/10.24425/mms.2018.124885

Jacek Jakubowski received his Ph.D. from the Military University of Technology, Warsaw, Poland, in 2000. He is currently an Associate Professor and the Vice Dean of the Faculty of Electronics at the Military University of Technology. His research activities focus on digital signal and image processing, data mining and deep learning methods in metrology, biometric and biomedical applications.